



# Determination of the onset of yielding and the Young's modulus after a change in the loading direction

Roman Norz<sup>1</sup> · Simon Vitzthum<sup>1</sup> · Maximilian Gruber<sup>1</sup> · Lorenz Maier<sup>1</sup> · Joana Rebelo Kornmeier<sup>2</sup> · Emad Maawad<sup>3</sup> · Fabuer R. Valencia<sup>4</sup> · Steffen Gerke<sup>4</sup> · Michael Brüning<sup>4</sup> · Wolfram Volk<sup>1</sup>

Received: 10 January 2024 / Accepted: 29 February 2024  
© The Author(s) 2024

## Abstract

The onset of plastic deformation is an important parameter for an accurate description of the flow curve and the Young's modulus. Determining the actual physical start of flow is already experimentally challenging for classic sheet metal materials. In addition to the experimental challenge, the onset of flow depends on numerous parameters such as strain rate, temperature and forming history. Non-proportional load paths in particular can significantly influence the onset of flow. Three different materials, a micro-alloyed steel HC340LA, a dual-phase steel CR330Y590-DP and an aluminium alloy AA6016-T4 are investigated in this publication. The physical onset of flow of the materials is determined at three different pre-strain levels as well as without and with a change in the load direction. Temperature-based approaches are used for this purpose. In-situ synchrotron diffraction is used to validate the results obtained. Those results can help to improve existing material models and springback prediction. Such models rely on material parameters that are as accurate as possible.

**Keywords** In-situ diffraction · Onset of yielding · Non-proportional load path

## Introduction

The results of a finite element simulation are only as good as the input parameters. If the material parameters are determined incorrectly, the real material behaviour can only be mapped inadequately. Particularly in complex multi-stage forming operations, a material model must be able to replicate the hardening behaviour as accurately as possible. In particular, the transition from the elastic to the plastic range after non-proportional load paths has been analysed in detail in numerous publications. Lian et al. [1] has summarized the following phenomena:

- Reduction of the yield strength also known as the Bauschinger effect
- Increased hardening rate at the beginning of the second loading step
- Stress-overshoot at the beginning of reloading
- Stress stagnation at the initial stage
- Permanent softening behaviour

Which phenomena occurs is dependent on many influences such as the material itself, the pre-forming level, the load case of the different loading steps and others. Tarigopula et al. [2, 3] has investigated the mechanical behaviour of a dual-phase steel DP800 after uniaxial pre-forming at different pre-forming levels. The elastic–plastic transition is affected the most if a tensile load case occurs for the reloading step, while a shear load case leads only to marginal changes of the material behaviour. Also the pre-forming level and the angle of the change in the loading direction plays a significant role in the elastic–plastic transition after reloading [4, 5]. The higher the change in the loading direction and the higher the pre-forming level, the more the elastic–plastic transition is affected. These findings were also found by Larsson et al. [6] for the dual-phase steels DP600 and DP1200. All these dual-phase steels revealed a

✉ Roman Norz  
roman.norz@utg.de

<sup>1</sup> Chair of Metal Forming and Casting, Technical University of Munich, Garching, Germany  
<sup>2</sup> Heinz Maier-Leibnitz Zentrum (MLZ), Technical University of Munich, Garching, Germany  
<sup>3</sup> Institute of Materials Physics, Helmholtz-Zentrum Hereon, Geesthacht, Germany  
<sup>4</sup> Institut für Mechanik und Strukturanalyse, University of the Bundeswehr Munich, Neubiberg, Germany

reduction of the yield strength after reloading. But not only dual-phase steels are affected. Also low carbon steels [7], or extra deep drawing quality steels [8, 9] are influenced. These softer steels tend to show a stress-overshoot at the beginning of the experiment if a change in the loading direction of more than  $45^\circ$  occurs. For aluminium alloys the studies of Barlat et al. [10] revealed a permanent softening behaviour for an AA1050-O after a uniaxial pre-forming followed by  $45^\circ$  simple shear experiment. For this aluminium alloy the change in the loading direction leads to a change in the material response. If the change in the loading direction is above  $45^\circ$ , a transient hardening behaviour and plastic instability is found [11]. For an AA6016, Manopulo et al. [8] have found, that the yield strength is reduced at the beginning but follows the flow curve of the initial material well after a certain plastic deformation. The AA5754 H111 aluminium alloy showed a permanent hardening behaviour after a change in the loading direction [1]. Again, the uniaxial pre-forming influenced the material the most. In general, the material, the amount of the change in the loading direction, the pre-forming level and the stress state of the loading steps are crucial parameters for the material behaviour under reloading.

As the stress–strain curves often show a very smooth transition with almost no linear elastic area, the determination of the Young's modulus is difficult. The Young's modulus is required to determine the yield strength according to the standard [12]. Therefore, more sophisticated methods to determine the onset of yielding were developed. Müller and Pöhlandt [13] as well as Banabic and Huetnik [14] used an infrared thermo-couple positioned above the center of the cruciform specimen to determine the yield loci of sheet metals. During the elastic regime the temperature of the material is reduced due to the increase in volume of the specimen. In the plastic regime, most of the work is converted into heat, leading to an increase in the temperature of the specimen. The temperature minimum is referred to as the onset of yielding. This method has been further improved by Vitzthum et al. [15]. At the time of the temperature minimum, an equilibrium between the elastic and the plastic deformation is reached. This means, in order to reduce the temperature decrease, internal energy has to be converted into heat. This leads to the conclusion, that at the temperature minimum,

plastic deformation has already occurred. Therefore, the onset of yielding is the deviation of the temperature signal from linearity. To validate the hypothesis, in-situ diffraction experiments have been conducted using an HC260Y steel. It was shown, that the physical onset of yielding is accurately described by the proposed method [16].

In this study, tensile tests with pre-formed specimens are conducted at the German Electron Synchrotron (DESY). The three materials, HC340LA, AA6016-T4 and CR330Y590-DP are investigated using synchrotron diffraction experiments. The three chosen material represent a wide range of materials with different responses, such as permanent softening, stress-overshoot or a reduced yield strength due to the Bauschinger effect, to orthogonal loading. During the experiments the temperature of the specimens is recorded by a temperature sensor. Also diffraction patterns are acquired at a rate of 1 Hz. By combining the macroscopic temperature signal as well as the applied stress with the microscopic results, the onset of yielding can be accurately determined for specimens under orthogonal loading. The determined yield strength is compared to the classical methods of the standard ISO6892-1 and the temperature minimum method.

## Experimental setup

The investigated materials were a micro-alloyed steel HC340LA and an aluminium alloy AA6016-T4 with an initial thickness of 1 mm and a dual-phase steel CR330Y590-DP with an initial thickness of 0.8 mm, further referred to as DP600. The materials have a very different microstructure with different grain sizes and phases, see Fig. 1. While the two steels have a relatively small grain size, the aluminium alloy has a grain size of approximately  $40\ \mu\text{m}$ .

## Pre-straining of the materials

To create the non-proportional load paths, large specimens of the material were cut out and formed on a hydraulic press using an oversized Marciniak-tool [17], see Fig. 2a. The specimen geometry is optimized in order to ensure that the maximum strains occur in the centre of the

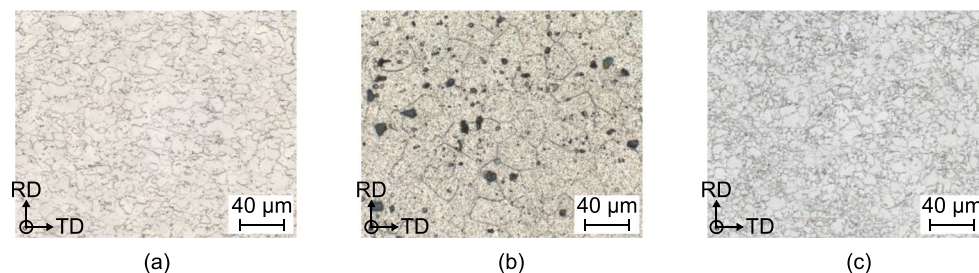


**Fig. 1** Microstructure of the HC340LA **a**, the AA6016-T4 **b** and DP600 **c**

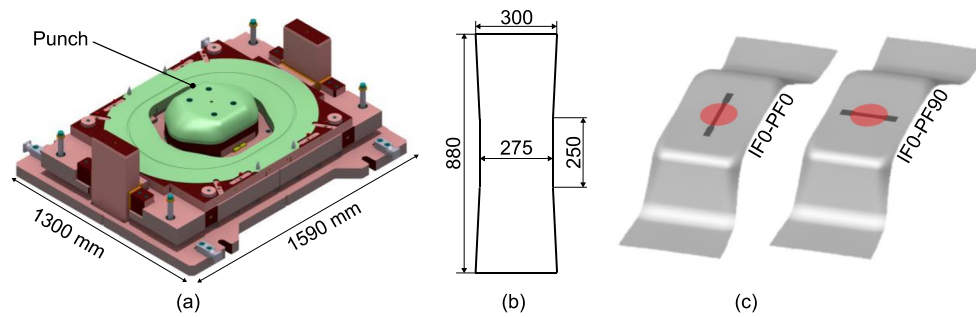


**Fig. 2** Modified Marciniak tool **a**, specimen geometry **b** and specimen notation and cut out process **c**

specimen. The width in the central area (250 mm length) is hence reduced from 300 to 275 mm, see Fig. 2b. The strains are measured by an optical measurement system using a grid which has been applied onto the specimens by etching prior to the pre-forming process. The rotation of the specimen is done by a simple rotation of the cut out geometry, see Fig. 2c. The initial loading direction is parallel to the rolling direction of the material. The specimens with no change in the loading direction are depicted as IF0-PF0 specimens, meaning that the initial forming (IF) and the post-forming (PF) are under  $0^\circ$  to the initial rolling direction. The orthogonal specimens are depicted as IF0-PF90, indicating a change in the loading direction by  $90^\circ$  in the post-forming step. The specimen geometry was of the shape H with a width of 12.5 mm, as mentioned in the standard DIN 50125 [18].

Three different pre-forming levels are selected. Next to the initial state, two different pre-forming levels at a maximum principal strain of approximately  $\epsilon_{pre} = 0.05$  and  $\epsilon_{pre} = 0.1$  are chosen. In order to proof that the pre-forming using the Marciniak tool leads to similar results as the tensile test, the strain evolution of the tensile test is compared to different pre-forming levels introduced by the Marciniak tool. The strain measurement during the tensile test is done by a DIC-System. The two different methods to pre-form the specimens lead to similar results, see Fig. 3. For the HC340LA steel, the pronounced yield strength can be clearly seen (Fig. 3a).

### Evaluation of the onset of yielding and the diffraction experiments

The effects of non-proportional load paths on the macroscopic scale are captured by the load cell, an applied strain gauge and the temperature sensor PT1000. To capture the microscopic effects, synchrotron diffraction experiments were carried out at the German Electron Synchrotron (DESY). These experiments allow the assessment of lattice strains.

For the tensile tests, a special test rig for in-situ diffraction experiments was used, shown in Fig. 4a. A detailed description of the tensile test rig can be found in [19]. To clamp the specimens, clamping jaws with four screws were used instead of wedge jaws. The four screws on each clamping jaw allowed a torque controlled clamping of the specimens. In comparison to wedge clamps, any slipping or movement of the specimens during the experiment can be avoided. A constant strain rate of  $0.00015 \text{ s}^{-1}$  was chosen for all materials to allow a detailed view of the elastic–plastic transition. Strain was measured using a strain gauge placed just above the centre of the specimen. This is necessary because the synchrotron beam hits the material in the central area of the sample, see Fig. 4b. A load cell mounted inside the test rig recorded the forces during the experiment. A PT1000 thermometer, see Vitzthum et al. [16] for details, was attached to the specimens just below the centre of the specimen to measure the temperature change throughout the experiment,

**Fig. 3** Comparison of the strain evolution in the tensile test and the Marciniak tool for HC340LA **a**, DP600 **b** and AA6016-T4 **c**. The further investigated pre-forming levels are marked with an arrow

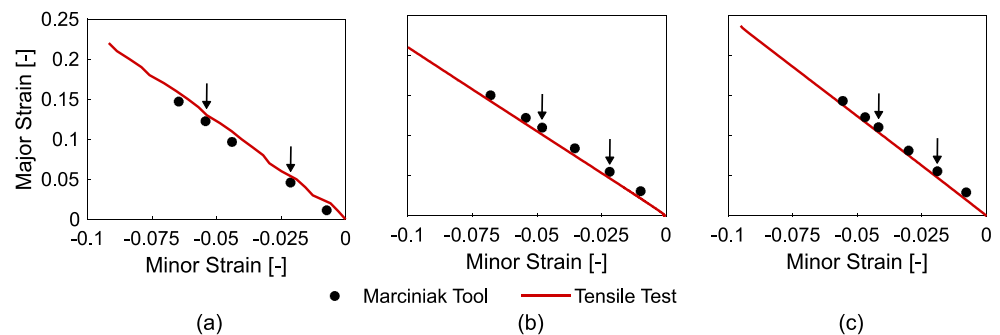
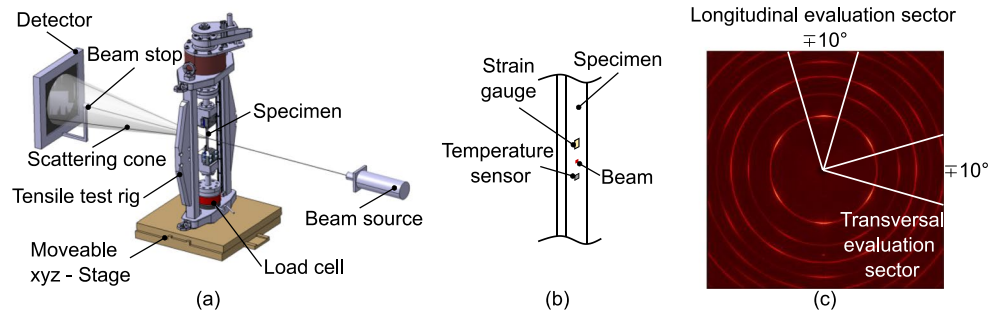


**Fig. 4** Experimental setup at the DESY **a**, Positions of the different sensors and the beam on the specimens **b**, diffraction pattern of the diffraction experiments **c**



see Fig. 4b. The HBM QuantumX data acquisition system was used to acquire the strain, load and temperature signals at a measurement frequency of 100 Hz. An air conditioning system kept the measurement room at a constant temperature throughout the experiments. The experiments started after the temperature signal had stabilised. Therefore, the samples have the same temperature as the ambient air and the clamping jaws. This reduces the thermal conduction effects. Due to the small changes in the temperature signal during the loading of the specimens of less than 1 K, the thermal conduction and thermal radiation are not taken into account. The correct mounting of the PT1000 sensor onto the specimen is much more critical.

The synchrotron beam had a wavelength of  $0.14235 \text{ \AA}$  and a beam size of  $0.7 \times 0.7 \text{ mm}^2$ . A Perkin Elmer XRD 1621 flat panel detector was used. This detector has  $2048 \times 2048$  pixels with a pixel size of  $200 \times 200 \text{ }\mu\text{m}^2$ . The detector spacing was set to 1062 mm in order to obtain a sufficient number of Debye–Scherrer rings. The setup allows a measurement frequency of 1 Hz for the diffraction experiments. A standard Lanthanhexaboride LaB6 sample with the same thickness as the tensile test samples was used to determine the misalignment and the sample to detector distance. To control the position of the beam on the sample throughout the experiment, the tensile test rig was moved at half speed by an XYZ positioning stage in the opposite direction to the

tensile loading direction. This allows the acquisition of the diffraction patterns of the same area throughout the experiment. A schematic representation of the experimental setup is shown in Fig. 4a.

The diffraction experiments are evaluated in two sectors oriented in the longitudinal direction, parallel to the loading direction, and in the transverse direction (see Fig. 4c). A sector with an angle of  $\pm 10^\circ$  was chosen for each direction. These sectors were integrated using the Fit2D software developed by Hammersley [20]. The resulting peak profiles were transferred to the AFit software where lattice planes (110), (200), (211), (220) and (310) were evaluated for the steels. For the aluminium alloy the lattice planes (111), (200), (220), (311), (400) and (331) were evaluated. The different lattice planes are chosen because of the different lattice structure of the materials. The steels have a body-centered cubic (bcc) structure while the aluminium alloy has a face-centered cubic (fcc) structure. The different 2D-profiles can be seen in Fig. 5a and b.

For peak fitting, a standard Gaussian function was sufficient for the investigated materials, as the processes investigated were mainly caused by microstrains, see Strunz et al. [21]. One main factor influencing the results significantly is the grain size of the material. Within the investigated volume (beam size multiplied by the material thickness), a sufficient amount of grains has to be present. The aluminium alloy

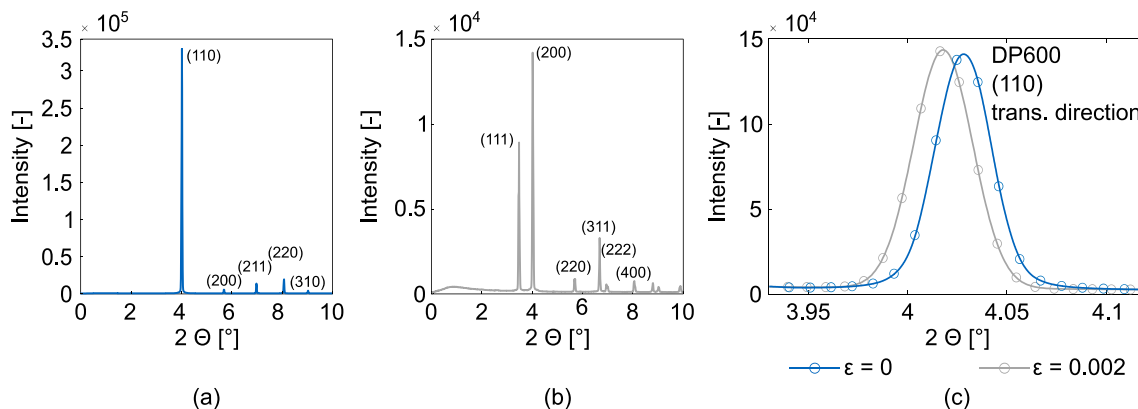
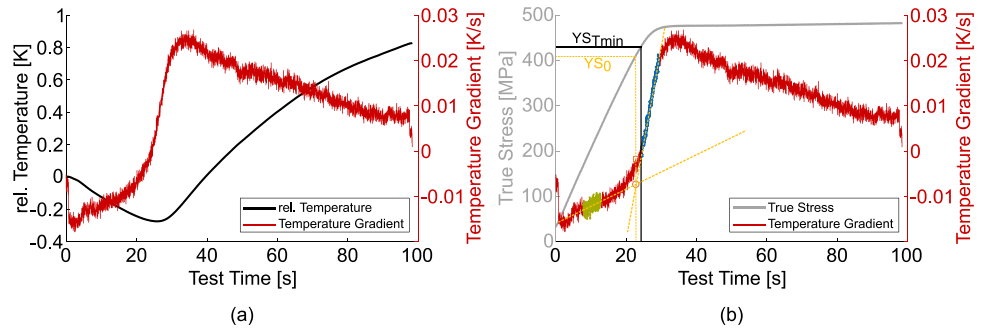


**Fig. 5** 2D-profile of a steel **a** and an aluminium sample **b** and the peak shift during loading in transversal direction **c**

**Fig. 6** Temperature signal of a tensile test sample during loading **a** and the evaluation of the two temperature-based methods **b**



with its grain size of approximately 25  $\mu\text{m}$ , see Fig. 1b is at the upper limit of the microstructure which can be investigated successfully. Materials with an even larger grain size are not well suited for such this experimental setup.

The specific lattice strains are determined by calculating the atomic spacing  $d_{hkl}$  using Bragg's law [22]:

$$n\lambda = 2d_{hkl}\sin(\theta), \tag{1}$$

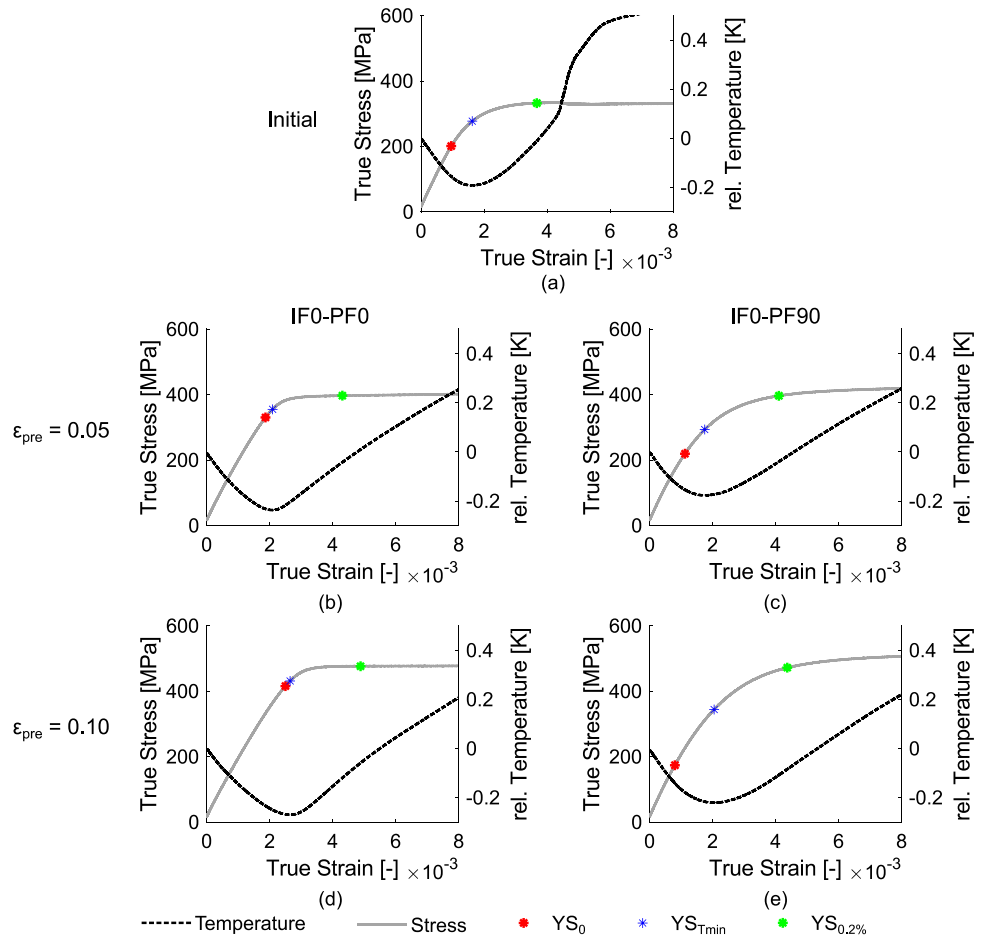
where  $n$  is an integer number,  $\lambda$  is the wavelength of the beam,  $\theta$  is the angle between the beam and the lattice plane and  $d_{hkl}$  is the atomic distance. The specific lattice strains are then related to the initial atomic distance  $d_{hkl}^0$  according to [23, 24]:

$$\epsilon_{hkl} = \frac{\sin(\theta_{hkl}^0)}{\sin(\theta_{hkl})} - 1 = \frac{d_{hkl} - d_{hkl}^0}{d_{hkl}^0}. \tag{2}$$

During the elastic regime, a linear increase of the lattice strains takes place. The slope of the increase is dependent on the Young's modulus of the lattice plane, the diffraction elastic constant (DEC). With the onset of deviation from the linear elastic behaviour, plastic deformation takes place and no further increase in the lattice strain is observed [25].

Three different methods were used to determine the onset of yielding. First, the classical method using Young's modulus according to the German standard DIN EN ISO 6892-1, represented as  $YS_{0.2\%}$ , which represents the yield strength at

**Fig. 7** Yield strength of the HC340LA steel for the initial material **a**, the  $\epsilon_{pre} = 5\%$  IF0-PF0 **b** and IF0-PF90 **c** specimens and the  $\epsilon_{pre} = 10\%$  IF0-PF0 **d** and IF0-PF90 **e** specimens



0.2% plastic strain. The other two methods are based on the thermoelastic effect. This effect describes the decrease in temperature during elastic tension caused by the change in volume of the specimen. This change is caused by the Poisson's ratio, which is approximately 0.3 for steel materials and 0.33 for aluminium in the elastic regime [26]. During plastic deformation, the temperature rises again due to the energy released, most of which is dissipated as heat. This effect was used by Sallat [27] to determine the onset of yielding in tensile tests. In order to assess the onset of yielding for more complex load cases, Müller [13] improved the measurement system so that it could be used in combination with a cruciform specimen. The yield strength under multiple loading conditions was determined using the cruciform specimen. Both researchers used the temperature minimum as the onset of yield. This method is also used and is referred to as  $YS_{T_{min}}$  in this study in accordance with [16]. Vitzthum et al. [16] also took into account that plastic deformation occurs prior to  $YS_{T_{min}}$ , as demonstrated by microstructural correlations. Based on this, the onset of the deviation from the linear decrease in temperature is taken as the onset of yielding. This deviation from linearity due to heating of the specimen is caused by plastic deformation. The stress at the time of deviation from linearity is called  $YS_0$ , as there is zero plastic deformation in the material at this

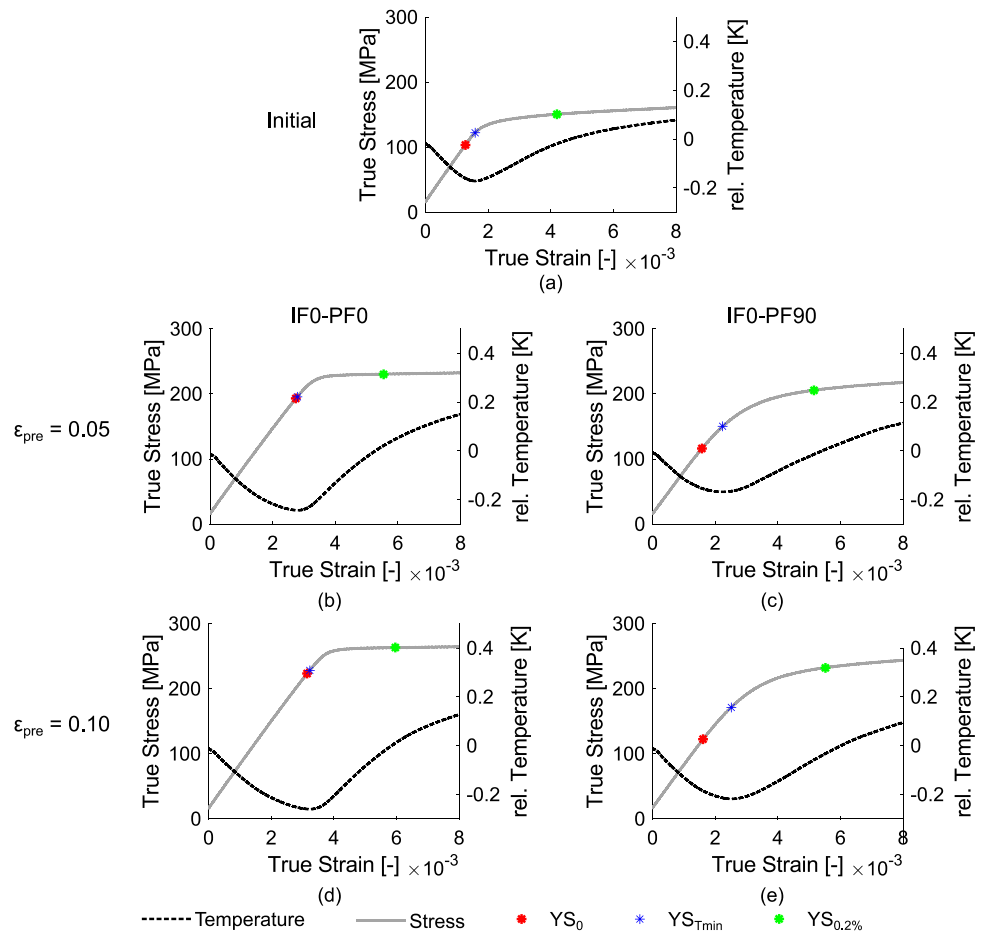
time. The derivative of the temperature signal is calculated to determine the onset of the non-linearity, see Fig. 6a. Two linear regression lines are then fitted to the area, one after the minimum of the temperature derivative (green section in Fig. 6b) and the other around the temperature minimum where the derivative is zero (steep increase in slope, blue section in Fig. 6b). An angle bisecting the intersection of the two lines gives the parameter  $YS_0$ . A more detailed description of this method can be found in Vitzthum et al. [16].

## Experimental results

### Onset of yielding

Figure 7 shows the onset of yielding for HC340LA steel. The yield strength of the temperature based methods is always below  $YS_{0.2\%}$ , regardless of the preformed state or loading direction. However, the temperature based methods are more influenced by preforming. When there is no change in loading direction, see the IF0-PF0 specimens in Fig. 7b and d,  $YS_0$ ,  $YS_{T_{min}}$  and  $YS_{0.2\%}$  move closer together, this effect is also found by other researchers [16, 28]. The temperature signal shows a sharper transition between the elastic

**Fig. 8** Yield strength of the aluminium alloy AA6016-T4 for the initial material **a**, the  $\epsilon_{pre} = 5\%$  IF0-PF0 **b** and IF0-PF90 **c** specimens and the  $\epsilon_{pre} = 10\%$  for the IF0-PF0 **d** and IF0-PF90 **e** specimens



and plastic regimes. The IF0-PF90 samples show a different behaviour. Here the three methods move further apart. The  $YS_0$  parameter is significantly lower than the  $YS_{0.2\%}$  parameter. This is due to a rounder temperature signal. This behaviour is also observed for the other steel, DP600. The results for the DP600 steel are shown in Fig. 12 in the Appendix. Both steels show a transient hardening behaviour after reloading for the IF0-PF0 specimens. For the IF0-PF90 specimens, a smooth elastic–plastic transition is visible in the stress–strain curve followed by a stress overshoot.

In Fig. 8 shows the onset of yield for the aluminium alloy AA6016-T4. The aluminium alloy shows a similar behaviour to the two steel materials. However, the differences between the three methods are generally smaller. For the IF0-PF90 specimens, the differences are also smaller compared to the steel grades. The aluminium alloy displayed a permanent softening behaviour for the IF0-PF90 specimens. The IF0-PF0 specimens showed a transient hardening behaviour at the first stage of reloading and followed the initial stress–strain curve well after a certain deformation. The increase in temperature signal is lower for the aluminium grade, mainly due to the lower strength of the material. The higher the strength of the material, the more work has to be done. As most of the work

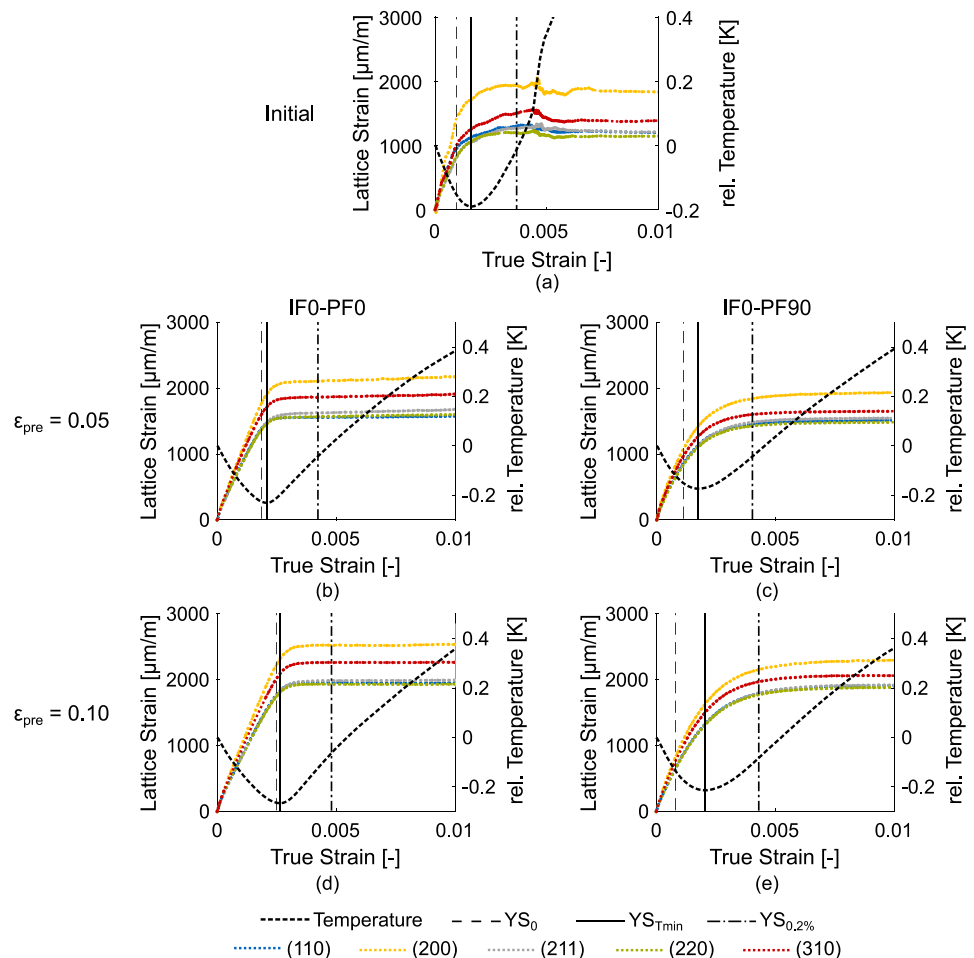
is converted into heat, the higher the strength of the material, the higher the temperature rise of the material.

### Lattice strains

The results of the three methods to determine the onset of yielding differ quite significantly. While the classical  $YS_{0.2\%}$ —method lead to an increase in the yield strength of all specimens after pre-forming, the temperature-based methods lead to an increase in the yield strength for the IF0-PF0 specimens. For the IF0-PF90 specimens, on the other hand, a decreasing yield strength is determined. To validate the obtained results, the lattice strains of different lattice planes are further investigated. Due to the limited experimental time at DESY, only one experiment per configuration is carried out.

The deformation behaviour of the lattice plane is in general similar to the behaviour on the macroscopic scale. During the elastic regime, the atomic distance is increased, leading to an increase in the lattice strain. After the onset of plasticisation no further increase can be observed as the atomic distance has reached its maximum and any further deformation leads to plastic deformation. For the HC340LA

**Fig. 9** Lattice strains of the HC340LA steel for the initial material **a**, the  $\epsilon_{pre} = 5\%$  IF0-PF0 **b** and IF0-PF90 **c** specimens and the  $\epsilon_{pre} = 10\%$  IF0-PF0 **d** and IF0-PF90 **e** specimens



steel, the lattice strains are shown in Fig. 9, while for the DP600 the results are shown in the Appendix in Fig. 13.

For the initial material (Fig. 9a) the pronounced yield strength of the material is clearly visible in the lattice strains. The lattice plane (200) shows the highest elastic formability, caused by the lowest DEC [29]. The lattice planes (110) and (220) are multiples of each other. Therefore, the two curves lie at top of each other and also have the highest DEC. The clear transition from the elastic to the plastic regime for the IF0-PF0 specimens can be observed, see (Fig. 9b and d and Fig. 13b and d). This is in good agreement with the sharp change in the temperature signal and the stress–strain curves. The DP600 steel even shows a lattice strain overshoot similar to the stress–strain curves. For the IF0-PF90 specimens (Fig. 9c and e and Fig. 13c and e), the transition between the elastic and plastic is not as clearly detectable. The smooth transition leads to the conclusion that some grains of a specific lattice plane tend to yield earlier than others, leading to the smooth transition. The first plastic deformation is nevertheless in good agreement with the yield strength determined by  $YS_0$ . At the time of  $YS_0$  the lattice strain of the individual planes start to differ from linearity.

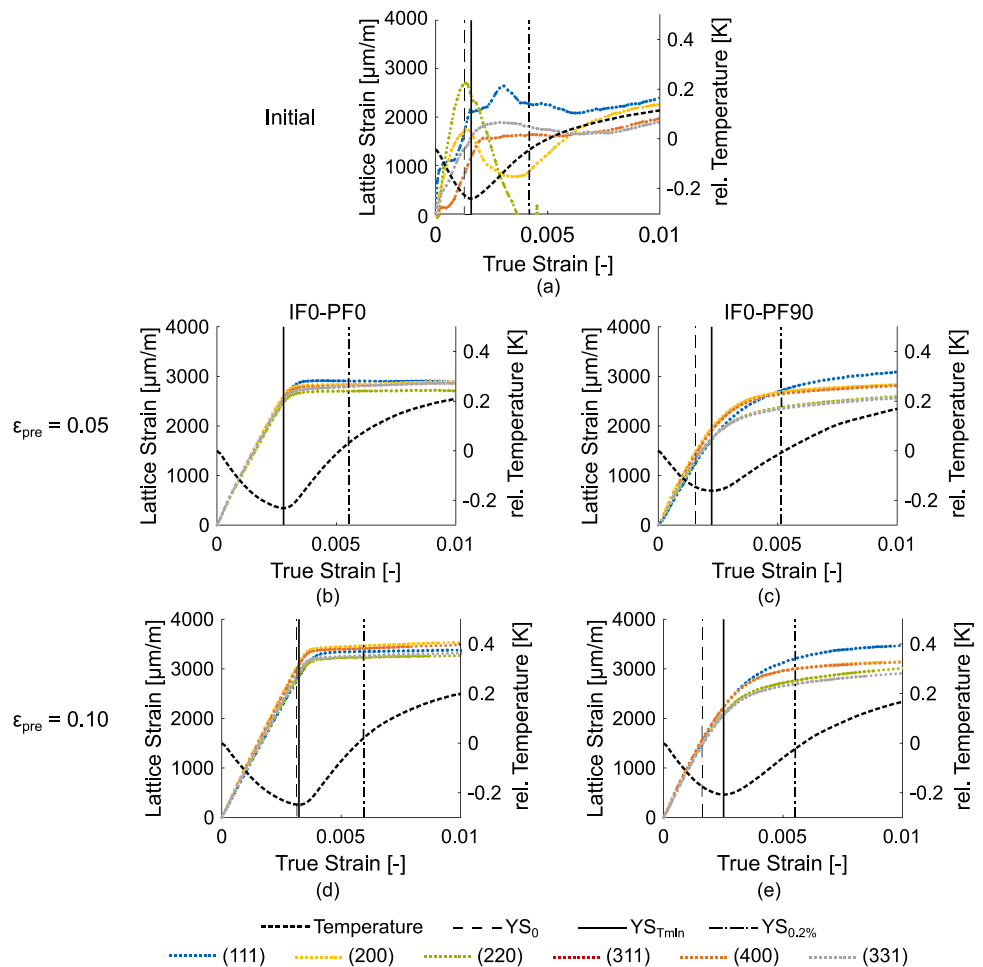
For the aluminium alloy AA6016-T4, the initial state shows a large scattering of the lattice planes, see Fig. 10a. This is caused

by the fact, that the grain size of the material is rather large with approximately 40  $\mu\text{m}$ . In combination with the area of the beam, the number of individual grains which can be observed is low. This leads to a poor statistic and the large scattering of some lattice planes. For the pre-formed material, the grains have elongated in the tensile load direction and have a reduced width. Due to that, the number of grains which can be investigated has increased and the scattering is reduced. In general it can be seen, that the individual lattice planes have a similar DEC and have the same elasticity, which is in good agreement with findings of other researchers [30, 31]. As for the HC340LA, the elastic–plastic transition is clearly visible for the IF0-PF0 specimens (Fig. 10b and d). For the IF0-PF90 specimens again, a smooth transition is observed (Fig. 10c and e). The transition is not as smooth as for the two steel grades, which is in good agreement with the stress–strain curves and the temperature signal.

### Young’s modulus

One parameter which the determination of the yield strength is dependent on, is the Young’s modulus. According to the standard DIN EN ISO6892-1 the starting and endpoint for the linear regression are dependent on the yield strength [12].

**Fig. 10** Lattice strain of the aluminium alloy AA6016-T4 for the initial material **a**, the  $\epsilon_{pre} = 5\%$  IF0-PF0 **b** and IF0-PF90 **c** specimens and the  $\epsilon_{pre} = 10\%$  for the IF0-PF0 **d** and IF0-PF90 **e** specimens





As the yield strength, especially for the IF0-PF90 specimens, differs significantly, it is expected for the Young's modulus to differ as well. For the evaluation the linear regression is done in between 30 and 70% of the yield strength.

The IF0-PF0 specimen, see Fig. 11a, c and e, show a reduction of the Young's modulus regardless of the evaluation method of the yield strength. For the AA6016-T4 and the DP600 the results are almost identical for all three methods. The HC340LA, on the other hand, shows differences in the initial Young's modulus. This difference is caused by the smooth elastic-plastic transition, see Fig. 7a. The evaluation of the Young's modulus is therefore affected by the reduced slope of the stress-strain curve. This behaviour is also observed by other researchers and multiple models such as the Yoshida-Uemori model [32] or the Quasi-Plastic-Elastic model (QPE-model) [33] have been proposed to take this effect into account.

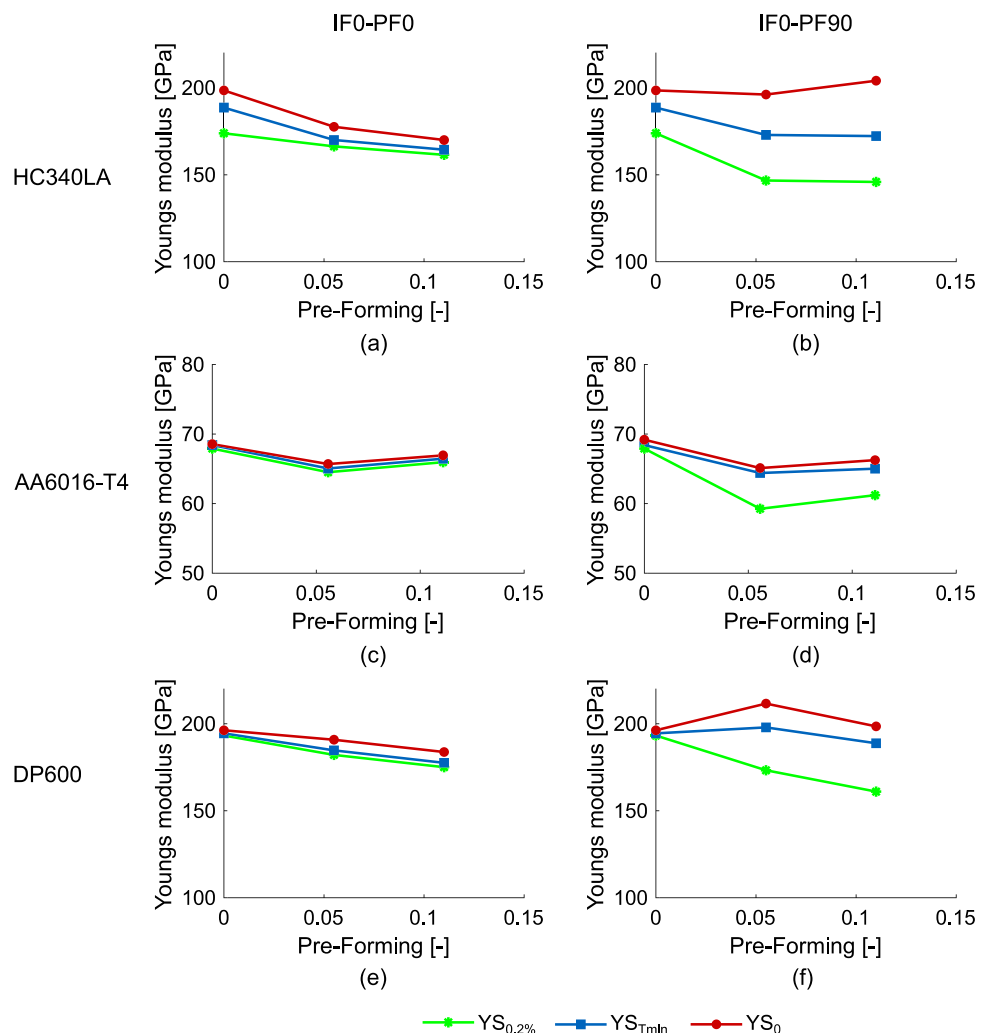
The IF0-PF90 specimens (Fig. 11b, d and f) show a different behaviour. While the  $YS_{0.2\%}$ -yield strength leads to a significant reduction in the Young's modulus the temperature-based methods lead to only a small reduction or even a slight increase in the Young's modulus. The reduction of the

Young's modulus when using the  $YS_{0.2\%}$  can be explained by the fact that the stress-strain curves of the IF0-PF90 specimens show a smooth elastic-plastic transition. During this smooth transition, some lattice planes already experience plastic deformation while others are still in the elastic regime. This non-linear behaviour of the stress-strain curves in combination with the increased yield strength  $YS_{0.2\%}$  leads to the reduction of the Young's modulus. The linear regression does not represent the material behaviour correctly. The temperature-based methods on the other hand have a lower yield strength and at that stage of the stress-strain curve a linear behaviour of the stress-strain curve is present.

### Conclusion

In this study, three materials namely a HC340LA, AA6016-T4 and a DP600, were subjected to tensile tests after pre-forming. The experiments were carried out in combination with multiple sensors and measuring devices. In order to capture the macroscopic effects the stress, the strain and the temperature

**Fig. 11** Young's modulus for the HC340LA **a** and **b**, the AA6016-T4 **c** and **d** and the DP600 **e** and **f**



were recorded. These data were combined with the microscopic results obtained by in-situ synchrotron diffraction in order to determine the physical onset of yielding after proportional (IF0-PF0) and non-proportional (IF0-PF90) loading. The results have shown, that the temperature-based methods can assess the onset of yielding for all investigated materials and load paths. The resulting yield strengths  $YS_0$  and  $YS_{Tmin}$  are reduced with increasing pre-forming level in combination with a change in the loading direction. This reduction is not observed when using the classical  $YS_{0.2\%}$ —method. These results were validated by the measurement of lattice strains. The plastic deformation of individual lattice planes correlates well with the  $YS_0$  – parameter. The temperature-based methods are a suitable method to determine the onset of yielding even for materials and load paths which show a very smooth elastic–plastic transition.

The determined parameters for the yield strength also lead to different Young’s modulus. While for the proportional load cases a reduction of the Young’s modulus is assessed, the non-proportional load cases show no decrease in Young’s modulus when the parameter  $YS_{Tmin}$  or  $YS_0$  is

used. The classical method by using  $YS_{0.2\%}$  lead to a significant reduction of the Young’s modulus.

The findings of this study are especially interesting for springback simulations. Currently many models only take into account a reduction of the Young’s modulus with increasing strain. In order to address the non-linear behaviour of the material during orthogonal loading, complex material models such as the homogeneous anisotropic hardening model (HAH-model) [34, 35] are required to capture the effects on the stress–strain curve. For the evolution of the Young’s modulus, the existing models need to be modified to address the obtained findings that there was no reduction of the Young’s modulus found for the IF0-PF90 specimens. Lee et al. [36] have combined the HAH-model to capture the effects on the stress–strain curves and the QPE-model to capture the effects on the Young’s modulus for cyclic tensile loading and unloading. But the effects of a change in the loading direction on springback predictions have not yet been fully captured, see [37]. When taking the effects of non-proportional load paths on the Young’s modulus into account, this might lead to an increased accuracy of material models.

## Appendix 1. Additional experimental data

**Fig. 12** Yield strength of the DP600 steel for the initial material **a**, the  $\epsilon_{pre} = 5\%$  IF0-PF0 **b** and IF0-PF90 **c** specimens and the  $\epsilon_{pre} = 10\%$  for the IF0-PF0 **d** and IF0-PF90 **e** specimens

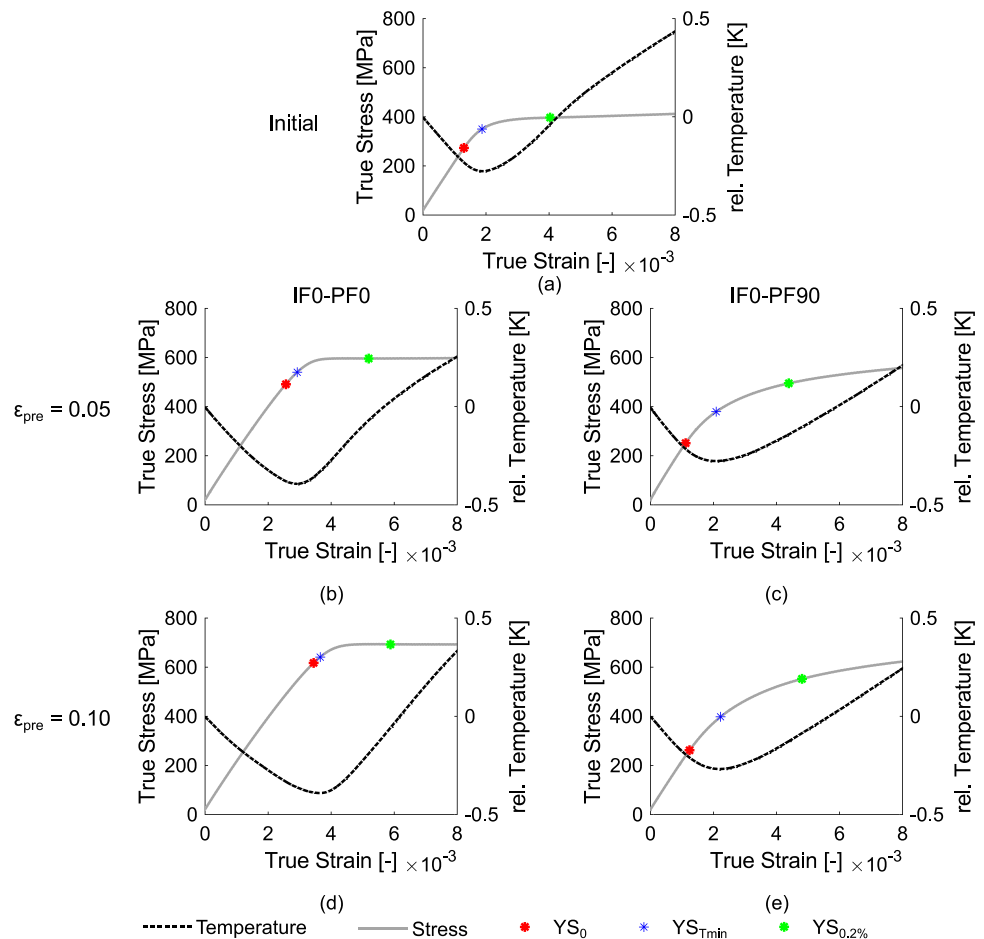
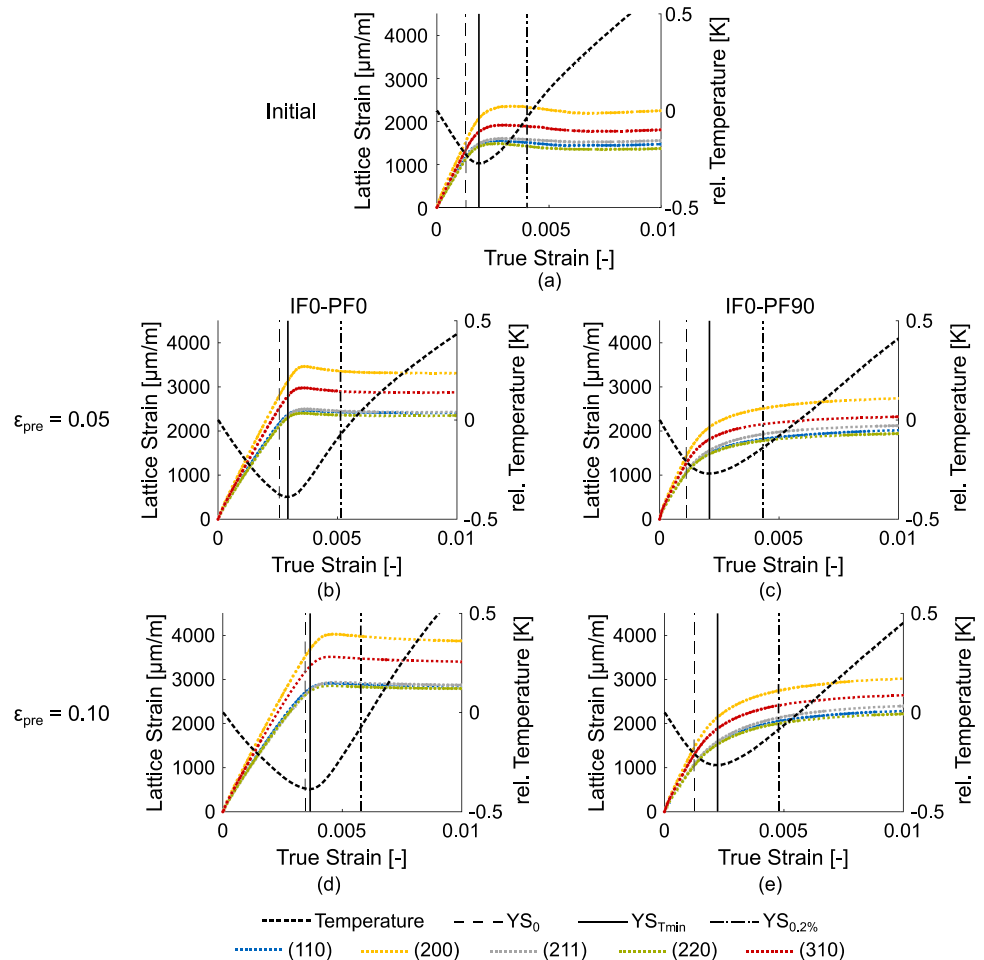


**Fig. 13** Lattice strain of the DP600 steel for the initial material **a**, the  $\epsilon_{pre} = 5\%$  IF0-PF0 **b** and IF0-PF90 **c** specimens and the  $\epsilon_{pre} = 10\%$  for the IF0-PF0 **d** and IF0-PF90 **e** specimens



**Acknowledgements** The authors would like to thank the German Research Foundation (DFG) for their financial support under the grant number 455960756. Furthermore, the authors would like to thank the team of Hereon Geesthacht for the measurement opportunity at the side station of the HEMS beamline at PETRA III synchrotron (DESY).

**Funding** Open Access funding enabled and organized by Projekt DEAL.

## Declarations

**Conflict of Interest** The authors declare that they have no conflict of interest.

**Open Access** This article is licensed under a Creative Commons Attribution 4.0 International License, which permits use, sharing, adaptation, distribution and reproduction in any medium or format, as long as you give appropriate credit to the original author(s) and the source, provide a link to the Creative Commons licence, and indicate if changes were made. The images or other third party material in this article are included in the article's Creative Commons licence, unless indicated otherwise in a credit line to the material. If material is not included in the article's Creative Commons licence and your intended use is not permitted by statutory regulation or exceeds the permitted use, you will

need to obtain permission directly from the copyright holder. To view a copy of this licence, visit <http://creativecommons.org/licenses/by/4.0/>.

## References

- Lian J, Liu W, Gastañares X et al (2022) Plasticity evolution of an aluminum-magnesium alloy under abrupt strain path changes. *Int J Mater Form* 15. <https://doi.org/10.1007/s12289-022-01692-6>
- Tarigopula V, Hopperstad OS, Langseth M et al (2008) Elastic-plastic behaviour of dual-phase, high-strength steel under strain-path changes. *Eur J Mech A Solids* 27:764–782. <https://doi.org/10.1016/j.euromechsol.2008.01.002>
- Tarigopula V, Hopperstad OS, Langseth M et al (2009) An evaluation of a combined isotropic-kinematic hardening model for representation of complex strain-path changes in dual-phase steel. *Eur J Mech A Solids* 28:792–805. <https://doi.org/10.1016/j.euromechsol.2008.12.004>
- Zaman SB, Barlat F, Kim J-H (2018) Deformation-induced anisotropy of uniaxially prestrained steel sheets. *Int J Solids Struct* 134:20–29. <https://doi.org/10.1016/j.ijsolstr.2017.10.029>

5. Qin J, Holmedal B, Hopperstad OS (2018) A combined isotropic, kinematic and distortional hardening model for aluminum and steels under complex strain-path changes. *Int J Plast* 101:156–169. <https://doi.org/10.1016/j.ijplas.2017.10.013>
6. Larsson R, Björklund O, Nilsson L et al (2011) A study of high strength steels undergoing non-linear strain paths—Experiments and modelling. *J Mater Process Technol* 211:122–132. <https://doi.org/10.1016/j.jmatprotec.2010.09.004>
7. Wen W, Borodachenkova M, Tomé CN et al (2016) Mechanical behavior of low carbon steel subjected to strain path changes: Experiments and modeling. *Acta Mater* 111:305–314. <https://doi.org/10.1016/j.actamat.2016.03.075>
8. Manopulo N, Hora P, Peters P et al (2015) An extended Modified Maximum Force Criterion for the prediction of localized necking under non-proportional loading. *Int J Plast* 75:189–203. <https://doi.org/10.1016/j.ijplas.2015.02.003>
9. Ha J, Lee M-G, Barlat F (2013) Strain hardening response and modeling of EDDQ and DP780 steel sheet under non-linear strain path. *Mech Mater* 64:11–26. <https://doi.org/10.1016/j.mechmat.2013.04.004>
10. Barlat F, Ferreira Duarte JM, Gracio JJ et al (2003) Plastic flow for non-monotonic loading conditions of an aluminum alloy sheet sample. *Int J Plast* 19:1215–1244. [https://doi.org/10.1016/S0749-6419\(02\)00020-7](https://doi.org/10.1016/S0749-6419(02)00020-7)
11. Vincze G, Butuc MC, Barlat F et al (2019) Strain path changes in aluminum. In: Proceedings of the 22nd international ESAFORM conference on material forming: ESAFORM 2019. AIP Publishing, p 160013. <https://doi.org/10.1063/1.5112710>
12. Deutsches Institut für Normung e. V (2020) Metallic materials – Tensile testing: Part 1: Method of test at room temperature(6892–1)
13. Müller W, Pöhländt K (1996) New experiments for determining yield loci of sheet metal. *J Mater Process Technol* 60:643–648. [https://doi.org/10.1016/0924-0136\(96\)02399-0](https://doi.org/10.1016/0924-0136(96)02399-0)
14. Banabic D, Huetink H (2006) Determination of the yield locus by means of temperature measurement. Proceedings of the 9th international ESAFORM conference on material forming: ESAFORM 2006:359–362
15. Vitzthum S, Hartmann C, Eder M et al (2019) Temperature-based determination of the onset of yielding using a new clip-on device for tensile tests. *Procedia Manuf* 29:490–497. <https://doi.org/10.1016/j.promfg.2019.02.166>
16. Vitzthum S, Rebelo Kornmeier J, Hofmann M et al (2022) In-situ analysis of the thermoelastic effect and its relation to the onset of yielding of low carbon steel. *Mater Des* 219:110753. <https://doi.org/10.1016/j.matdes.2022.110753>
17. Weinschenk A, Volk W (2017) FEA-based development of a new tool for systematic experimental validation of nonlinear strain paths and design of test specimens. In: Author(s), p 20009. <https://doi.org/10.1063/1.5007966>
18. Deutsches Institut für Normung e. V (2016) Testing of metallic materials - Tensile test pieces(50125)
19. Hoelzel M, Gan WM, Hofmann M et al (2013) Rotatable multifunctional load frames for neutron diffractometers at FRM II—design, specifications and applications. *Nucl Instrum Methods Phys Res Sect A* 711:101–105. <https://doi.org/10.1016/j.nima.2013.01.049>
20. Hammersley AP (2016) FIT2D : a multi-purpose data reduction, analysis and visualization program. *J Appl Crystallogr* 49:646–652. <https://doi.org/10.1107/S1600576716000455>
21. Strunz P, Lukás P, Neov D (2001) Data evaluation procedure for high-resolution neutron diffraction methods. *J Neutron Res* 9:99–106. <https://doi.org/10.1080/10238160108200131>
22. Bragg WH (1913) The Reflection of X-Rays by Crystals. *Nature* 91:477. <https://doi.org/10.1038/091477b0>
23. Rajagopalan S, Little AL, Bourke MAM et al (2005) Elastic modulus of shape-memory NiTi from in situ neutron diffraction during macroscopic loading, instrumented indentation, and extensometry. *Appl Phys Lett* 86. <https://doi.org/10.1063/1.1863437>
24. Qiu S, Clausen B, Padula SA et al (2011) On elastic moduli and elastic anisotropy in polycrystalline martensitic NiTi. *Acta Mater* 59:5055–5066. <https://doi.org/10.1016/j.actamat.2011.04.018>
25. Wang H, Wu PD, Tomé CN et al (2012) Study of lattice strains in magnesium alloy AZ31 based on a large strain elastic-viscoplastic self-consistent polycrystal model. *Int J Solids Struct* 49:2155–2167. <https://doi.org/10.1016/j.ijsolstr.2012.04.026>
26. Greaves GN (2013) Poisson’s ratio over two centuries: challenging hypotheses. *Notes Rec* 67:37–58. <https://doi.org/10.1098/rsnr.2012.0021>
27. Sallat G (1988) Theoretische und experimentelle Untersuchungen zum Fließverhalten von Blechen im Zweiachsigen Hauptspannungszustand. Dissertation, TU Karl-Marx-Stadt, 1988
28. Vitzthum S, Kornmeier JR, Hofmann M et al (2022) In-situ analysis of the elastic-plastic characteristics of high strength dual-phase steel. *Mater Sci Eng A* 857:144097. <https://doi.org/10.1016/j.msea.2022.144097>
29. Eigenmann B, Macherauch E (1996) Röntgenographische Untersuchung von Spannungszuständen in Werkstoffen. Teil III. Fortsetzung von Matwiss. und Werkstofftechn. Heft 3/1995, S. 148–160 und Heft 4/1995, S. 199–216. *Materialwissenschaft Werkst* 27:426–437. <https://doi.org/10.1002/mawe.19960270907>
30. Zhong ZY, Brokmeier H-G, Gan WM et al (2015) Dislocation density evolution of AA 7020–T6 investigated by in-situ synchrotron diffraction under tensile load. *Mater Charact* 108:124–131. <https://doi.org/10.1016/j.matchar.2015.09.004>
31. Zhang XX, Lutz A, Andrä H et al (2021) Evolution of microscopic strains, stresses, and dislocation density during in-situ tensile loading of additively manufactured AlSi10Mg alloy. *Int J Plast* 139:102946. <https://doi.org/10.1016/j.ijplas.2021.102946>
32. Yoshida F, Uemori T, Fujiwara K (2002) Elastic–plastic behavior of steel sheets under in-plane cyclic tension–compression at large strain. *Int J Plast* 18:633–659. [https://doi.org/10.1016/s0749-6419\(01\)00049-3](https://doi.org/10.1016/s0749-6419(01)00049-3)
33. Sun L, Wagoner RH (2011) Complex unloading behavior: Nature of the deformation and its consistent constitutive representation. *Int J Plast* 27:1126–1144. <https://doi.org/10.1016/j.ijplas.2010.12.003>
34. Barlat F, Vincze G, Grácio JJ et al (2014) Enhancements of homogenous anisotropic hardening model and application to mild and dual-phase steels. *Int J Plast* 58:201–218. <https://doi.org/10.1016/j.ijplas.2013.11.002>
35. Barlat F, Yoon S-Y, Lee S-Y et al (2020) Distortional plasticity framework with application to advanced high strength steel. *Int J Solids Struct* 202:947–962. <https://doi.org/10.1016/j.ijsolstr.2020.05.014>
36. Lee J, Lee J-Y, Barlat F et al (2013) Extension of quasi-plastic–elastic approach to incorporate complex plastic flow behavior – application to springback of advanced high-strength steels. *Int J Plast* 45:140–159. <https://doi.org/10.1016/j.ijplas.2013.01.011>
37. Lee S-Y, Yoon S-Y, Kim J-H et al (2023) Evaluation of loading-path-dependent constitutive models for springback prediction in martensitic steel forming. *Int J Mech Sci* 251:108317. <https://doi.org/10.1016/j.ijmecsci.2023.108317>

**Publisher's Note** Springer Nature remains neutral with regard to jurisdictional claims in published maps and institutional affiliations.